

Article

# Simulation of Marine Leisure Accidents Using Random-Walk Particle Tracking on Macro-Tidal Environment

Hyeon-Jeong Kim <sup>1</sup> and Seung-Won Suh <sup>2,\*</sup> 

<sup>1</sup> The Sea-Born eXperts Inc., Gunsan 54150, Jeollabuk-do, Korea; liswjd@gmail.com

<sup>2</sup> Department of Ocean Science and Engineering, Kunsan National University, Gunsan 54150, Jeollabuk-do, Korea

\* Correspondence: suh@kunsan.ac.kr; Tel.: +82-63-469-1713

**Abstract:** In the west coast of Korea (WCK), macro-tidal environments with wide tidal flats yield distinctive characteristics such as recursive tidal currents and tidal asymmetry. Here, we proposed an efficient search and rescue (SAR) computation method for WCK conditions (where bottom shapes affect nearshore sticking) using a finely resolved wet–dry circulation model. A random-walk particle tracking module (PTM) was applied to an unstructured finite element model to provide the SAR information needed to mitigate the consequences of marine leisure accidents. To capture the unique external forcing characteristics affecting the nearshore SAR case, sensitivity tests, which considered the characteristics of human bodies in particle representation, were performed on an idealized basin under typical external forcing. Furthermore, the effects of surface drag were included to represent real conditions more accurately. Our simulations showed that the accuracy of initial accident times for in situ mannequin floating tests (where several initial locations and times of accidents were used) directly affected the accuracy and effectiveness of SAR missions. However, to understand and predict the missing floating person in real time, additional intensive field experiments are required that account for the local geomorphological characteristics, external real-time temporal tides, and wind forcing incorporating extreme weather conditions.

**Keywords:** marine leisure accident; search and rescue; macro-tidal environment; wind factor; particle tracking model



**Citation:** Kim, H.-J.; Suh, S.-W. Simulation of Marine Leisure Accidents Using Random-Walk Particle Tracking on Macro-Tidal Environment. *J. Mar. Sci. Eng.* **2022**, *10*, 447. <https://doi.org/10.3390/jmse10030447>

Academic Editor: Alfredo L. Aretxabaleta

Received: 3 January 2022

Accepted: 15 March 2022

Published: 21 March 2022

**Publisher's Note:** MDPI stays neutral with regard to jurisdictional claims in published maps and institutional affiliations.



**Copyright:** © 2022 by the authors. Licensee MDPI, Basel, Switzerland. This article is an open access article distributed under the terms and conditions of the Creative Commons Attribution (CC BY) license (<https://creativecommons.org/licenses/by/4.0/>).

## 1. Introduction

Owing to increasing leisure populations engaging in diverse marine activities, unexpected accidents are inevitable at beaches or offshore. Moreover, increasing floating litter from discarding overland and marine garbage degrades the coastal environment and reduces the safety of aqua activities. In addition, frequent transport of crude oil sometimes causes a severe oil spill accident. Most of the west coast of Korea (WCK) consists of a macro-tidal environment with a mean spring tidal range of 3 to 9 m and a very shallow depth with a bottom slope of  $0.4\text{--}1.3 \times 10^{-3}$ , from the Mokpo located in the southwest to the Incheon in the middle of the Korean Peninsula (Figure 1). These authentic ambient coastal environments yield associated wide intertidal flats, strong tidal currents, and complex nonlinear tidal constituents. In addition, safety accidents during marine leisure near coastal areas exposed to dangerous conditions sometimes require search and rescue (SAR) operations by the Korean Coast Guard (KCG) to be conducted within the so-called “golden” time of rescue. Although such operations depend on the water temperature, KCG aims for an operating system through which they can arrive at the accident site within an hour for successful rescue operation and to accomplish the operation within 6 h in a normal situation to ensure survival. Floating materials on marine surfaces are treated as free drifts, that is, neutral particles, regardless of their shape and size, with randomness according to tidal currents and surface wind stresses. Thus, it is essential to understand and operate

SAR by particle movement with focus on ambient tidal conditions, especially in the WCK, where macro-tidal environments dominate, and surface wind stress during the accidents.

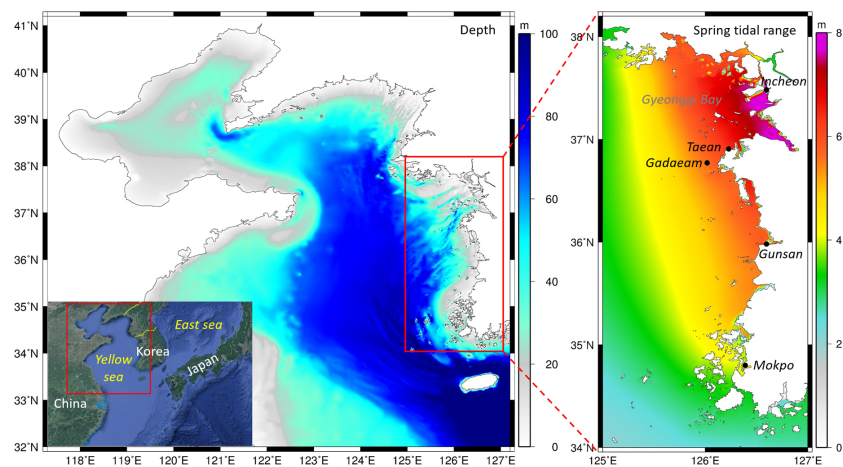


**Figure 1.** Map showing study area, WCK, with complex coastlines, shallow depth (bathymetry data from KorBathy30s [1]), and spring tidal range (computed as  $2[M_2+S_2]$ ).

According to KCG analyses, marine leisure safety accidents mostly occur on natural (i.e., offshore, nearshore, beaches, tidal-flat, and seashore rocks) and artificially treated coastal infrastructure (such as harbors, breakwaters, and bridges) during fishing, swimming, and diverse aquatic activities. The death toll resulting from annual marine accidents and natural (artificial) coastal areas was 378 (224) from 2017 to 2020 (Figure 2). The main reasons for safety accidents in artificial and natural environments are falling from coastal structures and drowning, isolation, and inability to escape due to rapidly rising tidal speeds in open tidal flats or very mild slope beaches. Figure 2 shows a high risk of death toll due to marine leisure activity scattered along the coast regardless of accident types. The local geomorphological environment sometimes dominates rescue operation; therefore, it should precisely capture not only the temporal hydrodynamic variants but also spatial characteristics of the high-risk area. With the use of appropriate real-time SAR operations, such safety accidents on both coastal infrastructures can be minimized. However, because the high tidal range causes a wide area of dry and rewetted conditions periodically, such peculiar cases should be moderately incorporated into SAR modeling systems.

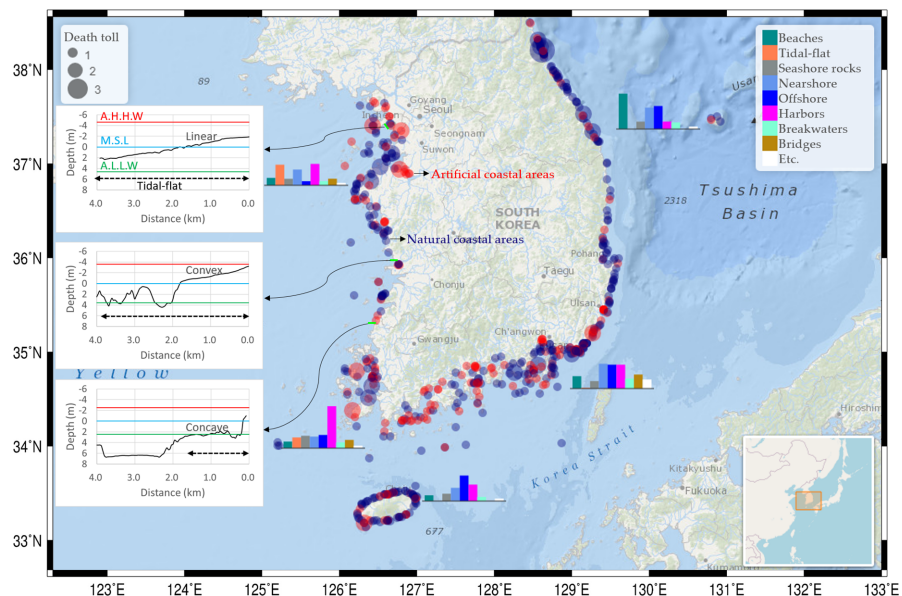


**Figure 2.** Coastal accidents depending on locations (indicated by different colors) around the Korean

Peninsula with death toll for subregional seas (bar chart) during 2017–2020. For selected coastal locations, typical three-bed sloping types are demonstrated with tidal ranges between approximately higher high water (AHHW) level and approximately lower low water (ALLW) level.

## 2. Background

Random-walk particle tracking models (PTMs) have been applied in diverse situations, such as identifying ocean and estuarine mixing mechanisms, by Bilgili et al. [2] and Büyükçelebi et al. [3]; modeling coastal debris to simulate floating debris from Malaysian Airlines Flight 370 [4]; simulating the oil spills induced by the Hebei Spirit accident in 2007 [5,6] and oil leakage from the sea bed in the Gulf of Mexico [7]; conducting SAR in maritime emergencies [8–11]; analyzing the tidal barrier effect [12]; simulating heated water discharge with buoyant particles [13] and fish larval transport [14,15]; and tracking marine plastics by using beaching mechanism [16] and marine litter drift [17–19]. Although these models account for various oceanic or coastal hydrodynamics, including tidal, wind, and atmospheric variations, only a few of the particle tracking analyses [2,3,16,20] consider wet and dry conditions. However, beaching and backwashing is rather important because trapped floating materials on the exposed tidal flat would not move offshore without sudden overwash events, such as a flood tide that transports them onshore, as in the macro-tidal environment of WCK. Thus, in this study, we explored some sensitivity particle tracking simulations that take into consideration the diverse forms of sloping bed profiles: linear, concave, and convex types (shown in Figure 2 for typical locations with tidal ranges), in a macro-tidal environment to highlight the materials of the different resultant trapping of floating bodies, including humans, from coastal marine leisure or safety accidents that may be missed by SAR. Previous studies [21,22] regarding marine drift include oil spills, lifeboat, human body, and marine litter in the form of styrofoam, plastic bottles, and broken plastic material [21,23–28], which introduce leeway drift simulation under wind conditions to determine the drifting location.

The classical techniques for modeling the transport of floating debris are only moderately successful owing to several unknowns or assumptions, as stated by Critchell et al. [29], such as the value of the wind drift coefficient, variability of the oceanic forcing and wind, resuspension of floating debris by waves, and poorly known relative contribution of floating debris from diverse sources. These problems are not restricted to marine debris, but tracking other floating objects using a numerical model.

In this study, marine leisure safety accidents and unexpected floating bodies under a macro-tidal environment with very mild onshore and offshore slopes on tidal flats were simulated using a random-walk PTM based on the coastal and ocean circulation model, Advanced Circulation (ADCIRC; [30]). Drifters on the sea surface can be moved by tidal currents and wind drags with respect to the floating type and shape, and further moving is induced by the leeway effect. Marine leisure accidents around coastal areas such as beaches, marinas, small ports, tidal channels, coastal rocks, and breakwaters, occur occasionally, and a prompt SAR operation is required to increase the possibility of locating drifting missing humans. The main objective of this study was to initiate and provide a scientific background (information) of SAR to the KCG. However, the unique physical characteristics of WCK and the wide range of tidal fluctuations hinder direct application approaches in simulating SAR events or predicting spills offshore [5,6].

In these numerical simulations, the constituents of small drifts and human bodies are mainly considered in the performance of neutral PTMs to extend an early warning system (EWS) for the storm season and provide real-time marine hazards induced by safe accidents during marine leisure activities and unexpected ship collision. The particle tracking scheme was applied to the existing EWS frame by ADCIRC + SWAN [31]. However, because of numerous unknowns underlying geophysical characteristics, we elucidated and identified the drifting mechanisms in a macro-tidal environment by testing sensitivity in a simplified basin of a representative case of WCK for bottom slopes, shape, turbulence dispersion, missing location (with respect to separating distance from the coast), and leeway coefficients

regarding floating materials. After the sensitivity tests, field verification with a mannequin drogue experiment was used to demonstrate the feasibility of the proposed approach.

### 3. Method

In this study, for the Eulerian circulation analysis, we adopted a depth-averaged two-dimensional finite element model, ADCIRC, to represent the complex coastal geometry of the WCK. It solved the generalized wave continuity equation, which is a modified form of the shallow water equations, and momentum equations on unstructured meshes in a Cartesian or spherical coordinate system. Under certain coastal hydrodynamic conditions, the Lagrangian passive particle tracking approach by introducing the random-walk method was incorporated.

The general discrete form of PTM [9,13,32] comprises the deterministic drift part and dispersion part with randomness, as shown in Equation (1) [32]:

$$\mathbf{X}_p(t + \Delta t) = \mathbf{X}_p(t) + \mathbf{A}(\mathbf{X}_p, t)\Delta t + \mathbf{B}(\mathbf{X}_p, t) \cdot \boldsymbol{\xi}(t)\sqrt{\Delta t}, \quad (1)$$

where  $\Delta t$  is the time step,  $\mathbf{X}_p(t)$  is the position of a particle at time  $t$ , and  $\mathbf{A}$  is a drift vector;  $\mathbf{B}$ , the displacement matrix, is a tensor defining the strength of dispersion, and  $\boldsymbol{\xi}(t)$  is a vector of independent, normally distributed random variables with zero mean and unit variance [32].

Generally, drift is replaced with tidal or ocean current. In this study, the influence of wind on particle movement was considered in the drift; thus, the drift vector can be expressed as shown in Equation (2) [17]:

$$\mathbf{A} = u_c + W_f \mathbf{u}_w, \quad (2)$$

where  $w_f$  is the windage coefficient and  $\mathbf{u}_w$  is the wind velocity 10 m above the sea.

#### 3.1. Sensitivity Tests to Identify Geomorphological Characteristics

In this study, to demonstrate the characteristics of the macro-tidal environment affecting particle movement, we used several sensitivity tests prior to real application by simply changing the bottom slope variations: linear, concave, and convex, within an idealized basin, as shown in Figure 3a. The simplified basin was set to represent the typical bottom geometry of WCK, as shown in Figure 2, near Incheon, Gunsan, and Mokpo. We tested particle release locations and the re-moving possibility due to the captured or beached objects on a tidal flat on a simplified coastal basin, as shown in Figure 3a.

To determine the macro-tidal hydrodynamic effects on PTM, a simplified basin of 25 km  $\times$  25 km, except for the tidal flat area, resolved with a regular spacing of 50 m (Figure 3a), was discretized with variable size grids forming 60,377 nodes and 120,500 elements. Open boundary forcing of the four major tidal constituents was prescribed to represent a typical macro-tidal environment.

By analyzing the bathymetry data of KorBathy30s [1], mean bottom slopes of  $0.4 \times 10^{-3}$  to  $1.3 \times 10^{-3}$  from the coast to offshore at selected sites for macro- and meso-tidal basins were extracted. In the numerical simulations for a simplified tidal basin, mild slopes and macro- to meso-tidal environments were used to capture the actual situations of the WCK from Gyeonggi Bay to the southernmost Korean Peninsula [33]. The external forcing function as amplitudes and phases extracted from NAO99.jb [34] of four major tidal constituents,  $M_2$ ,  $S_2$ ,  $K_1$ , and  $O_1$ , were applied along the open boundaries (Table 1). A simplified idealized tidal basin with mean slopes in conjunction with typical bottom types of linear, convex, and concave shapes were used to determine the relative responses against external forcing on particle movements. Different types of bottom slopes are shown in Figure 3b, and the simulated onshore–offshore velocity variations along the cross-section AA', as in Figure 3a, are plotted in Figure 3c.

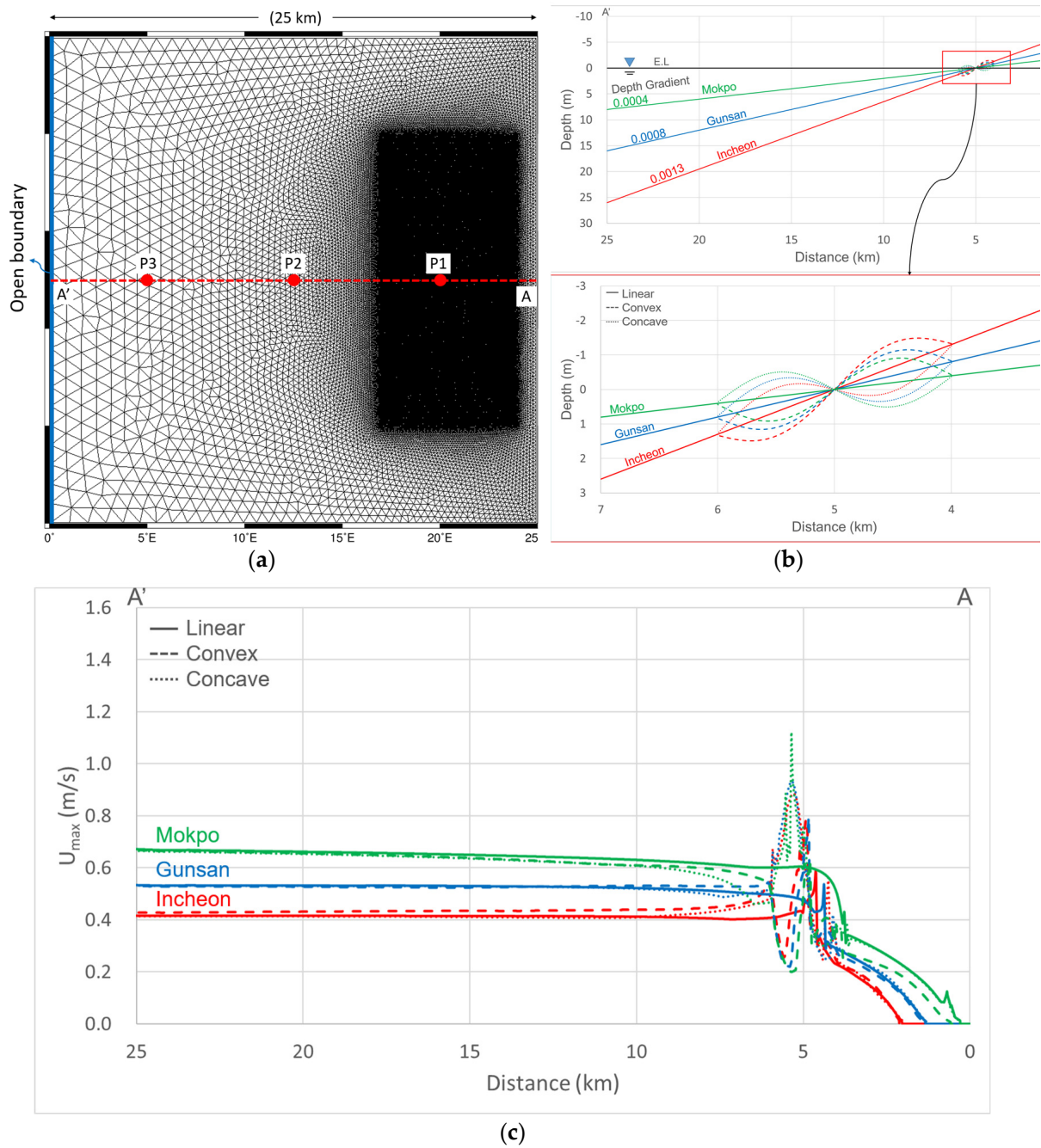


**Figure 3.** Simplified basin (a) for sensitivity tests, (b) bathymetry shapes at near the coast, and (c)  $x$ -directional maximum velocities along transect AA'.

**Table 1.** Tidal amplitude (m) applied at an open boundary representing macro-tidal and meso-tidal environments for a simplified case.

Constituents	Incheon	Gunsan	Mokpo
M <sub>2</sub>	2.57	2.04	1.43
S <sub>2</sub>	0.97	0.77	0.52
K <sub>1</sub>	0.39	0.34	0.32
O <sub>1</sub>	0.29	0.24	0.24

### 3.2. Wind Effect on Particle Movement

According to previous works [23,25,27,28], wind affects drifting objects by the leeway effect, regardless of the material (Equation (3)). In one instance, the drift due to leeway was approximately 25% greater than the drift due to the surface currents under the wind and current conditions [25]. As floating body ratio ( $A_{air}/A_{water}$ ) changes the traveling time, these relationships could be applied in simulating and finding floating locations.

$$\frac{U_{leeway}}{U_{wind}} \sim \sqrt{\frac{\rho_{air}C_D A_{air}}{\rho_{water}C_W A_{water}}}, \quad (3)$$

where,  $U_{leeway}$  is the leeway drift speed (m/s),  $U_{wind}$  is the wind field at 10 m height of wind speed (m/s),  $\rho_{air}$  is the air density ( $\text{kg}/\text{m}^3$ ),  $\rho_{water}$  is the sea water density ( $\text{kg}/\text{m}^3$ ),  $C_D$  is the wind drag coefficient,  $C_W$  is the current drag coefficient, and  $A_{air}$  and  $A_{water}$  are the area of the over-water and submerged parts of the drifting objects, respectively [23].

Because the unknowns change with respect to the floating material and its portion, it is difficult to apply a single or constant value. Nevertheless, in the first attempt of wind effects on the numerical simulation, a wind-induced shear effect factor,  $w_f$ , was incorporated. Moreover, detailed coefficients of parameters should be withdrawn in field tests considering variant wind forcing.

In this study, sensitivity tests of wind factor were performed by 20% increase or decrease compared to the base value of 0.03 to identify the importance of the surface wind effects under the macro-tidal environment. Leeway effect was not actually fully accounted because of nearshore floating consideration in this study; however, the effect may act as an important factor in offshore simulation. Thus, the leeway effect should be investigated and tested in future studies. In addition, in case of storm events, the combined effect of current and wave should be applied to account for the wave effect using a tightly coupled model of circulation and wave such as ADCIRC + unSWAN [7,31].

### 3.3. In Situ Mannequin Tracking and Numerical Discretization

Floating human body tracking for in situ experiments was performed using three embedded global positioning systems (GPS) equipped on mannequins, as shown in Figure 4. Among the tests, the tracking interval was set to every 5 s during 25 June 2021 02:40–08:07 (UTC), which corresponds to flooding tides from low to high, to capture the actual conditions of a typical WCK environment. The total floating distance was 6.2 km heading to the northeast direction along the coastal line showing a maximum dispersion coefficient of  $1.27 \text{ m}^2/\text{s}$  with a mean value of  $0.08 \text{ m}^2/\text{s}$ . The dispersion coefficient was calculated through the square product of relative separating distances ( $\Delta d_i$ ) of each mannequin for every elapsed time span  $\Delta t$ , i.e.,  $\Delta d_i^2/\Delta t$ . This information was applied to sensitivity tests in an idealized basin.

In the numerical simulation of the actual coastal area, we considered the representative area of the mid-WCK, even among the areas at risk of coastal safety accidents. Many coastal aquatic activities have expanded in the surrounding areas. In addition, in these areas, it is easy to examine the behavior of a human body or pollutants in the water caused by coastal safety accidents; thus, a floating mannequin experiment was performed to understand floating body movements in real situations. In particular, it has the advantage of being able to practically examine and simulate whether free random movements of particles, a characteristic of coastal intertidal zones, are adsorbed, stuck, or resurfaced, depending on the tidal environment.

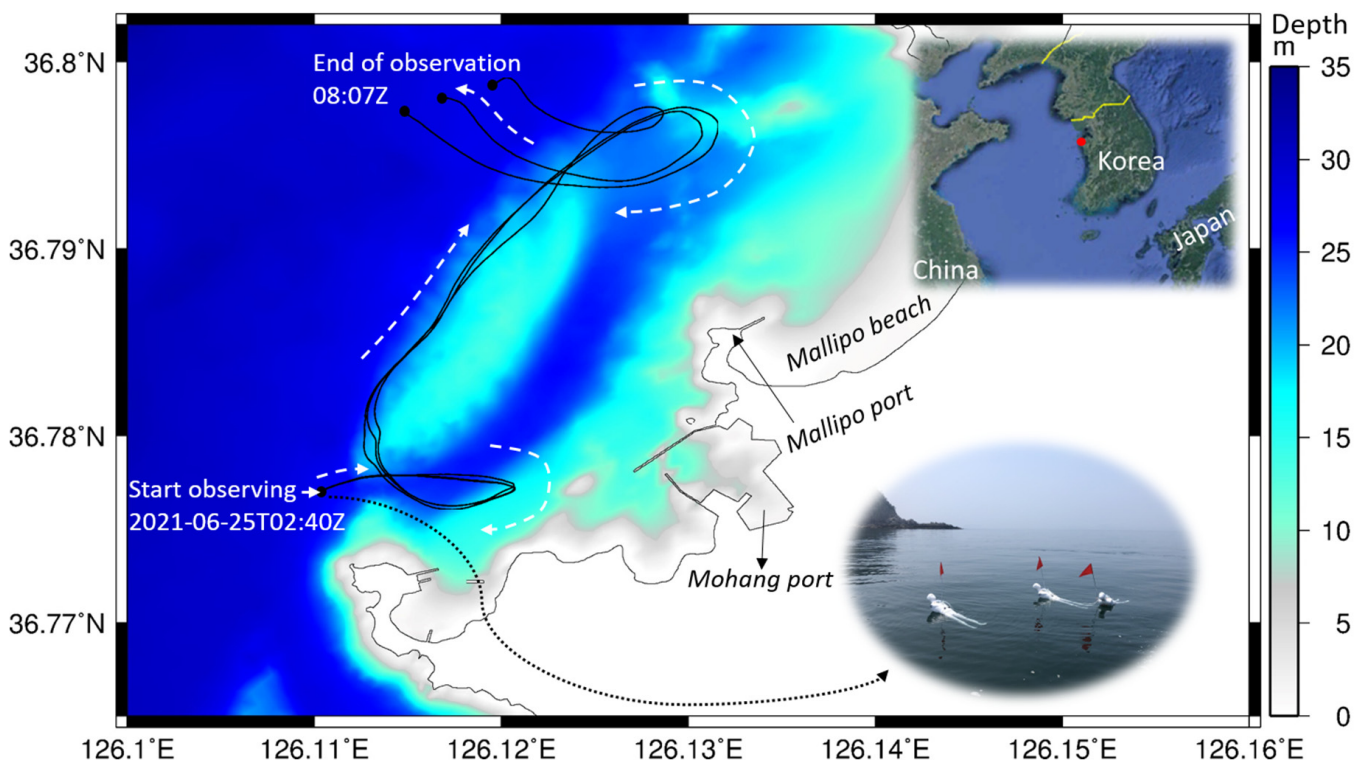


**Figure 4.** Map showing in situ mannequin drogue experiment near a beach in WCK.

To reproduce the behavior of a drowning body in the actual coastal area, the North Western Pacific Grids having 258 k vertices (NWP-G258k) [31] grid system, which was introduced in the precise EWS of typhoon storm surges covering the northwest Pacific Ocean and finely resolved in a coastal area of shallow depth, as in the WCK, was used. In addition, the detailed depth by KorBathy30s [1] was interpolated along with the grid details in the mid-WCK. As discussed earlier in the idealized tests, because the bottom topography of water depth in the offshore direction greatly affects the movement of coastal floats, it is important to describe the bottom topography based on accurate water depth data of the target area. The minimum grid was resolved as approximately 10 m in the Mallipo intertidal zone in which marine safety accidents were markedly higher than those in other zones, while grids of ~25 m were used in discretization where the mannequin tracking experiment was performed. Because the region of interest has been finely resolved based on a reference grid of approximately 258,000, the total number of nodes in the grid increased to 278,206, and the number of elements was 522,935 (Figure 5). The dispersion coefficient calculated through the mannequin tracking experiment was applied to the particle tracking simulation. For the meteorological information, the Japan Meteorological Agency meso-scale model was initially applied to provide the locality of wind forcings via assimilation during 15 June 2021 to 28 June 2021, but such external wind stress forcing can be reproduced using the ADCIRC + SWAN model taking into account the weather information. The simulated weather and tidal results were applied as an external force to the random-walk PTM. At the starting point of mannequin tracking,  $10^3$ – $10^5$  particles assuming the human body were released and the rescue positions were determined in terms of probabilistic search area.

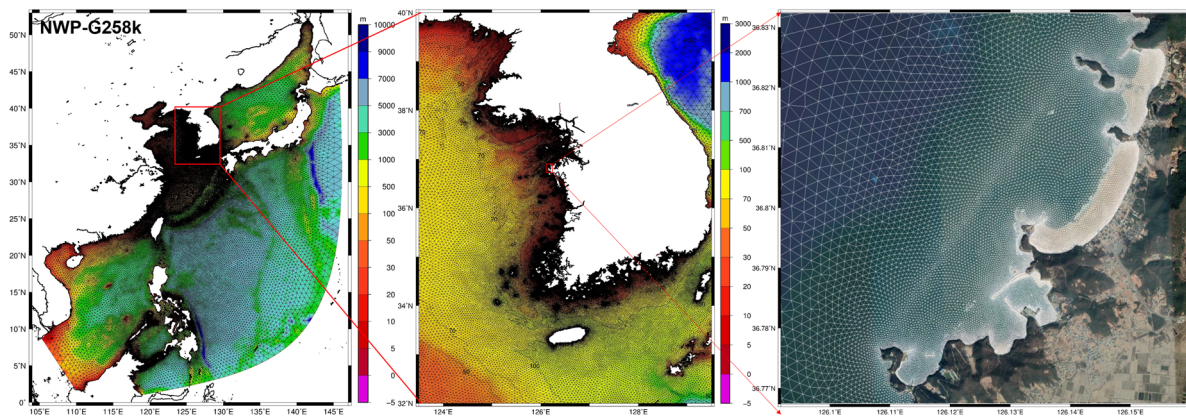


**Figure 5.** Unstructured grid system, NWP-G258k, with locally refined grid for field experiment verification.

#### 4. Results and Discussion

Any marine numerical simulations inevitably have limitations in terms of the numerical methods of approximation, considering external environment forcing, mapping the geomorphological characteristics in discretization, and computing accuracy. Though the unknowns can be somewhat minimized by applying state-of-the-art schemes, models with appropriate sensitivity tests for ambiguity can have additive effects on the understanding of natural chaos. For this purpose, we tested the sensitivities as described in the previous section, and the results are discussed below.

##### 4.1. Effects of Bottom Slope and Shape in PTM

The bottom slope of the meso-tidal basin is twice that of the macro basin, while the external tidal forcing is greater within the macro basin. To determine the particle movement and associated sensitivities in different tidal environments, particle release locations were set at the outer (P1), mid (P2), and inner parts (P3) of the basin (Figure 6 and Video S1). The released particles were tracked every hour to measure the total behavior of advection with respect to tidal movement and dispersion, and to determine the most probable locations of particle clusters. As expected, the dispersed distances increased as time elapsed after the initial release instances.

Fluctuating patterns in the macro-tidal basin differed according to the release locations, i.e., it was higher at the inner location (P1) adjacent to the coast but decreased slowly in farther locations (P2 and P3), as shown in Figure 6. Meanwhile, in the meso-tidal basin, the fluctuating amplitudes did not show distinct patterns with respect to the source locations. Moreover, bottom shapes greatly affect the inner location (P1) of the macro-tidal basin, but the effects decreased at P2 and P3. In the meso-tidal basin, the bottom shape effect was insignificant regardless of source release points.

To understand particle movements, the maximum dispersion distances were calculated in accordance with the bottom shapes. The results showed that macro-tidal environments enhance the random movement of particles compared to meso-tidal basins. Maximum distances released at the P1 location were 3.67 (3.95), 6.74 (10.52), and 5.62 (7.98) km for Incheon (Mokpo) tidal conditions in accordance with linear, convex, and concave shapes, respectively (Table 2). External environments with meso-tidal conditions increased by 56.1% and 42.0% for convex and concave bottom shapes, respectively. Meanwhile, the particles released at P3 location, increased by 9.7% and 6.3% under the same conditions. This suggests that floating or lost materials, including human bodies, in beaches or tidal flats adjacent to shores can move wider than tidal excursion lengths. This suggests that the convex shape of the bottom geography directly affects the coastal buoyant particles. However, the linear bottom slope does not affect floating particle movement compared to

the uneven bottom shapes. Thus, the bottom topography, including wide tidal flats, need to be precisely described for effective SAR operations.

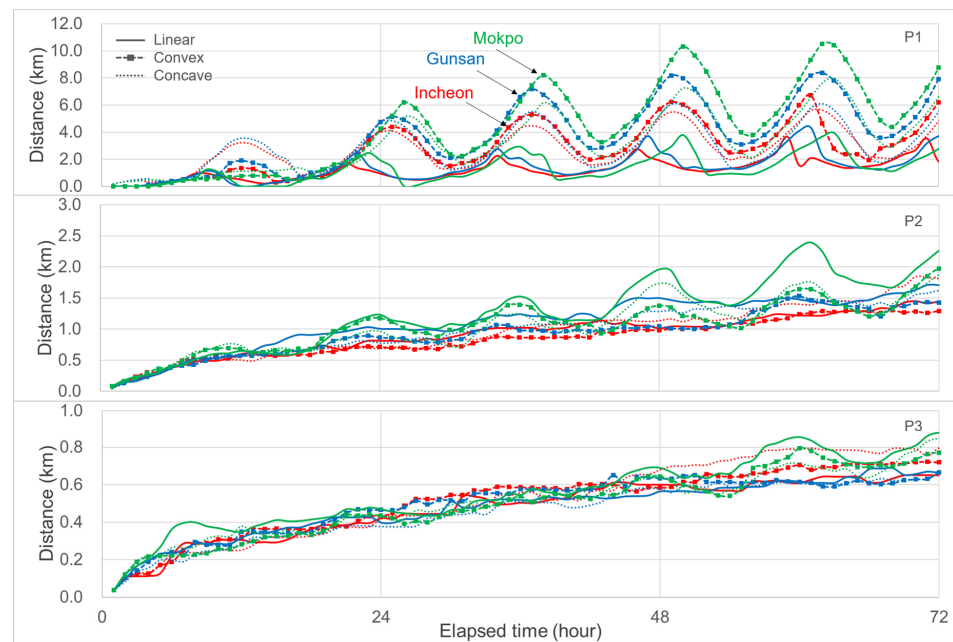


**Figure 6.** Temporal variation of fluctuating particle movement with respect to bottom shapes: linear, concave, and convex for macro- (Incheon) to meso-tidal (Mokpo) conditions.

**Table 2.** Average and maximum dispersion distance (km) in macro-tidal and meso-tidal environments according to the bottom slope shape.

Station	Bottom Slope Shape	Incheon		Gunsan		Mokpo	
		Ave.	Max.	Ave.	Max.	Ave.	Max.
P1	Linear	1.24	3.67	1.40	4.33	1.30	3.95
	Convex	2.77	6.74	3.76	8.36	4.37	10.52
	Concave	2.70	5.62	2.88	6.10	3.28	7.98
P2	Linear	0.91	1.45	1.10	1.71	1.25	2.40
	Convex	0.84	1.30	0.93	1.53	1.05	1.97
	Concave	0.96	1.84	0.99	1.62	1.04	1.87
P3	Linear	0.47	0.65	0.48	0.69	0.55	0.88
	Convex	0.51	0.72	0.50	0.57	0.49	0.79
	Concave	0.52	0.80	0.45	0.66	0.50	0.85

Based on numerical simulations, we found that the initial release location of floating particles was very important for understanding overall dispersive movements. In particular, under low tidal forcing in a meso-tidal basin, particles or buoyant materials lost adjacent to the coast could be stuck on tidal flats during flooding tides, and some of them resurface after high tide. This recursive pattern continues, and thus the number of remaining particles in coastal areas exponentially decreases. As a result, the final maximum dispersion length is much smaller than that of the macro-tidal basin.

Stuck and resuspended (beaching and backwashing) particles on the coast of tidal flats or marshes with respect to ascending or descending tides should be emphasized when modeling a marine rescue operation to successfully identify the golden time for SAR operations. This is because the imbalanced recursive patterns could mislead SAR teams away from traditional SAR activity offshore. Thus, in this study, we attempted to evaluate the existing ratio on coasts, that is, landed and attached floating materials. To demonstrate

onshore–offshore directional beaching and backwashing (landing and re-surfacing) effect of particles stuck on the tidal flats, a similar tidal environment in an idealized basin as listed in Table 1 was applied to obtain an insight while applying the model in an actual coastal environment. However, to simplify, the tidal phase was not considered on the open boundary shown in Figure 3a on a test basin. Thus, the results showed only minimal north–south excursion. We observed that approximately 66.6–98.4% of particles were stuck and did not resurface under the linear and convex bottom slope conditions (Figure 7). The landing and stuck particles in this special case might be caused by the complex effects of relatively short tidal variation and a small space to move back and forth. Thus, the resulting re-surfacing momentum eventually decreases.

#### 4.2. Contribution of Dispersion

Sensitivity tests relating turbulent flow strength represented by the dispersion coefficient were performed to understand the impact of coastal meteorological conditions on tidal flow. The WCK is usually affected by winter NW and summer SW winds with mean (maximum) velocities of 3.4 (16.3) and 2.5 (17.7) m/s, respectively. Although actual turbulence is affected by several parameters, it is difficult to define the horizontal dispersion coefficient as a constant or time-variant value. After the field experiment of mannequin drogue tests, the simplified basin could have 0.2–1.8, 2, 5, and 10 m<sup>2</sup>/s dispersion coefficients of sensitivities. Numerical tests were performed by adding or decreasing the coefficients with respect to a basis setting value of 1.0 m<sup>2</sup>/s, which was measured in the field experiment (Figure 8). As expected, the moving distances increased with elapsed time of particle release after a sudden injection at the P1 location. Particles moved up to 3.9 km under the basis condition of the normal case but increased (decreased) by 14.2–60.3% (60.8–66.2%) by considering 80% of the dispersion coefficient fluctuations. These results indicate that higher values of the dispersion coefficients are rather insensitive. In the previous PTM application on the WCK by Suh [13], a mean value of 10 m<sup>2</sup>/s was adopted. However, there were no sensitivity tests. Hinata et al. [16] applied the same order of horizontal diffusivity of 10 m<sup>2</sup>/s. Owing to the importance of dispersion coefficients, Bilgili et al. [2] and Jalón-Rojas et al. [35] tested the sensitivities for dispersion coefficient by considering 1–10 m<sup>2</sup>/s. In this study, the coefficients were set to vary according to the field experiment conditions.

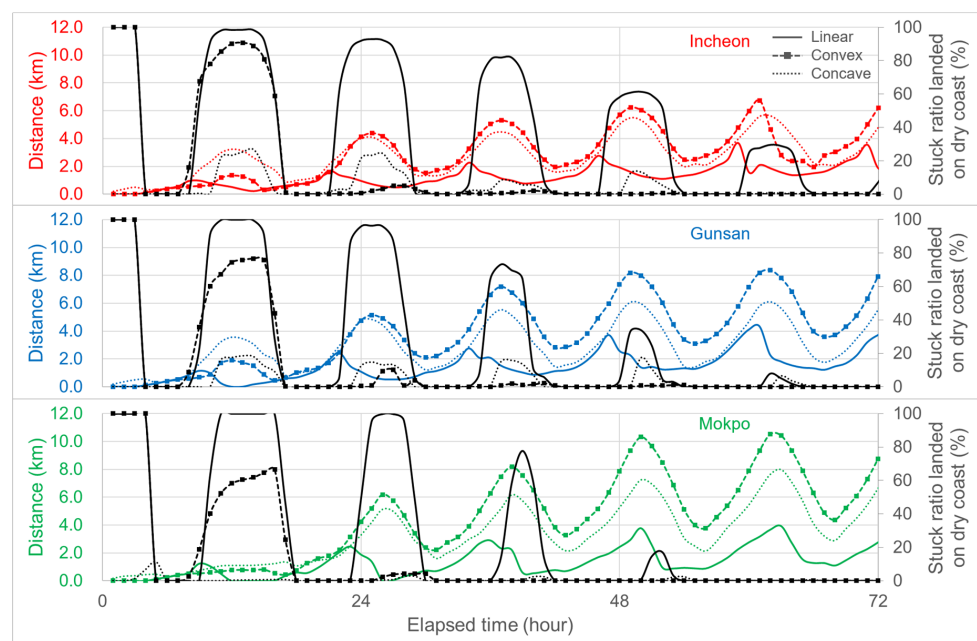


**Figure 7.** Temporal variation of particle movement (color solid and dotted lines) and stuck ratio landed on dry coast (black solid and dotted lines) with respect to bottom shapes.

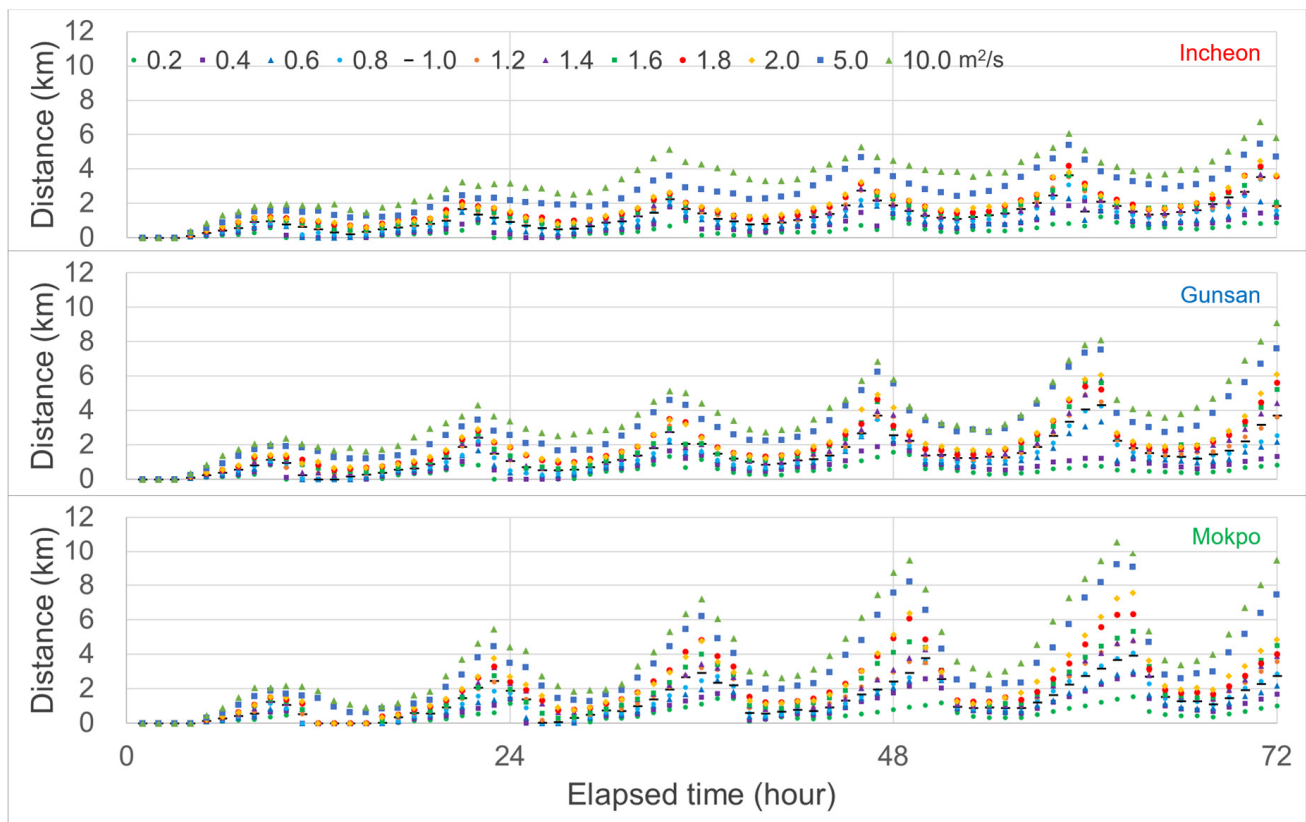


**Figure 8.** Temporal fluctuating particles regarding sensitivity tests for dispersion coefficients.

#### 4.3. Impacts of Particle Release Location Affecting Beaching and Backwashing

Most human accidents during leisure activities in coastal areas occur during the summer season when personal carelessness runs rampant, and there is impaired recognition of external weather variation or tidal rising speeds. Tidal rising speeds on mid WCK are especially fast (0.31–0.56 m/s) in meso- to macro-tidal areas with mean tidal slope of  $0.4 \times 10^{-3}$  to  $1.3 \times 10^{-3}$ . Unfortunately, there is insufficient information on the movement of floating human bodies for the high tidal regions on the tidal flat and beaches due to the very low-lying onshore–offshore characteristic. This hinders the accurate capture of traditional advection–dispersion associated with random-walk processes in marine trackings [4,6,22] due to the repeated or transitory behavior of attaching and resuspension on the coast under dry and wet conditions. Thus, the prevailing SAR operations offshore or at sea could not be directly applied, but such geophysical aspects should be taken into account in SAR analyses, particularly in particle tracking algorithms, to improve success rates. Therefore, we attempted to perform sensitivity tests to better understand coastal shores with very mild slopes and geological formulae, such as linear, concave, or convex shapes, by changing external tidal forcings for an idealized basin representing the WCK (Figure 9 and Video S1).

Our results showed that most of the particles released near the coast suffered landings on the shore during a flooding tide, but some of them remained even through the ebbing tide. However, when the release point is close to the offshore, the chance of landing and resurfacing is greatly reduced. Thus, in SAR operations that occur near the coast, such as beaches, rocks, and fishing harbors, careful attention should be paid to identifying possible rescue locations.

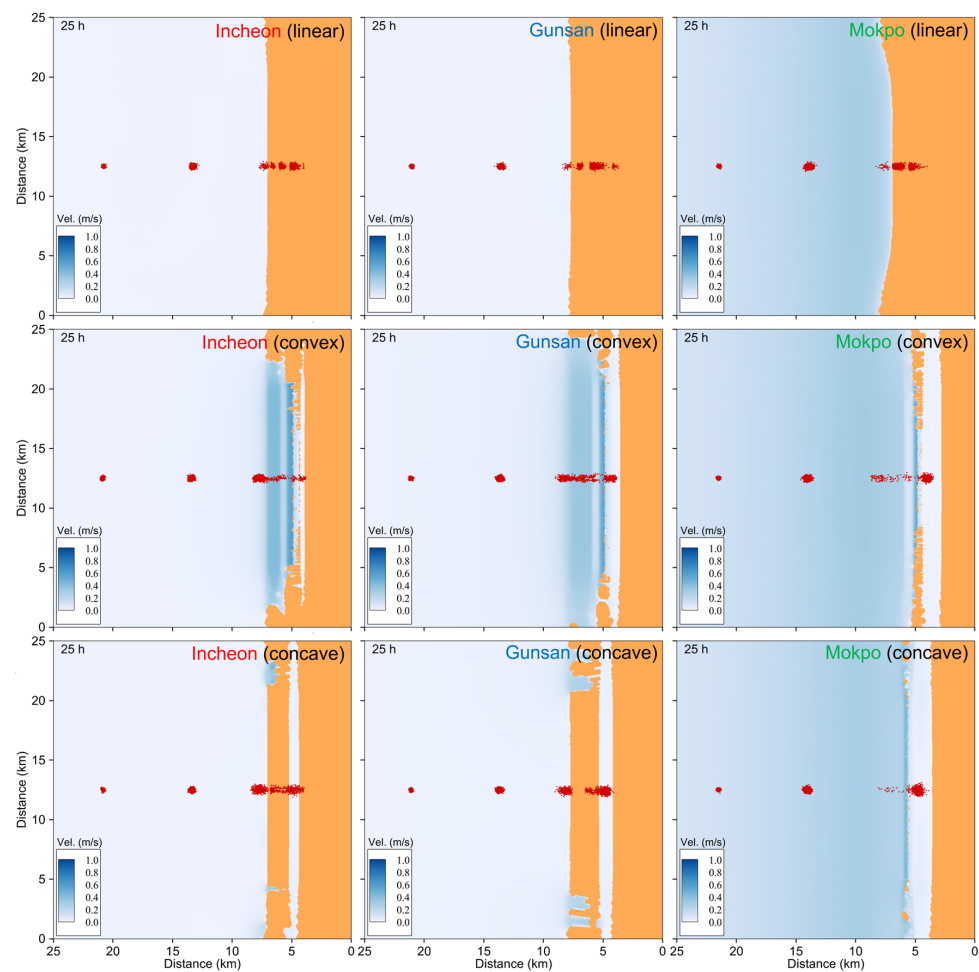


**Figure 9.** Particle behavior in the idealized wet-dry zone with respect to the bottom shape.

#### 4.4. Verification of Wind and Tide for In Situ Test

Marine conditions, such as tides and tidal currents, are the most influential factors in SAR operations at sea. From previous studies on coastal circulation and early warning of storm surges around the Korean coast [31,33], the circulation model ADCIRC was satisfactorily verified for observed tidal elevation and currents. However, to prove the validity of the ADCIRC circulation model applied in this specific case, the results reproduced using the numerical model during the mannequin observation period of the marine situation were compared with the recorded values of the Taean tidal station and the measured wind speeds near the in situ location. During the period corresponding to the experimental period, reproduced wind speeds were 0.9–2.5 m/s following the satisfactory overall trend of wind speed data (1.2–3.3 m/s) observed near stations. Nevertheless, the simulated tidal variation was very similar to the observed tides, with minimum observed (simulated) levels at low tide at  $-2.57$  ( $-2.61$ ) m, and maximum levels at high tide at 2.62 (2.69) m (Figure 10). The numerical simulation represented the real situation with satisfaction, so this was used to reproduce the movement of the human body as floating particles in the ADCIRC model. These results suggest that in situ experimental information introducing the leeway effect may be comparable with the simulated particle tracking results. Results of particle tracking with random-walk motion showed a dispersive pattern over time, as discussed in sensitivity tests in an idealized basin. The results were plotted with elapsed time from the source or missing location and animated, which is provided in Supplementary Materials, Video S2, to capture the time-dependent decreasing possibility of the search area with mannequin path lines.

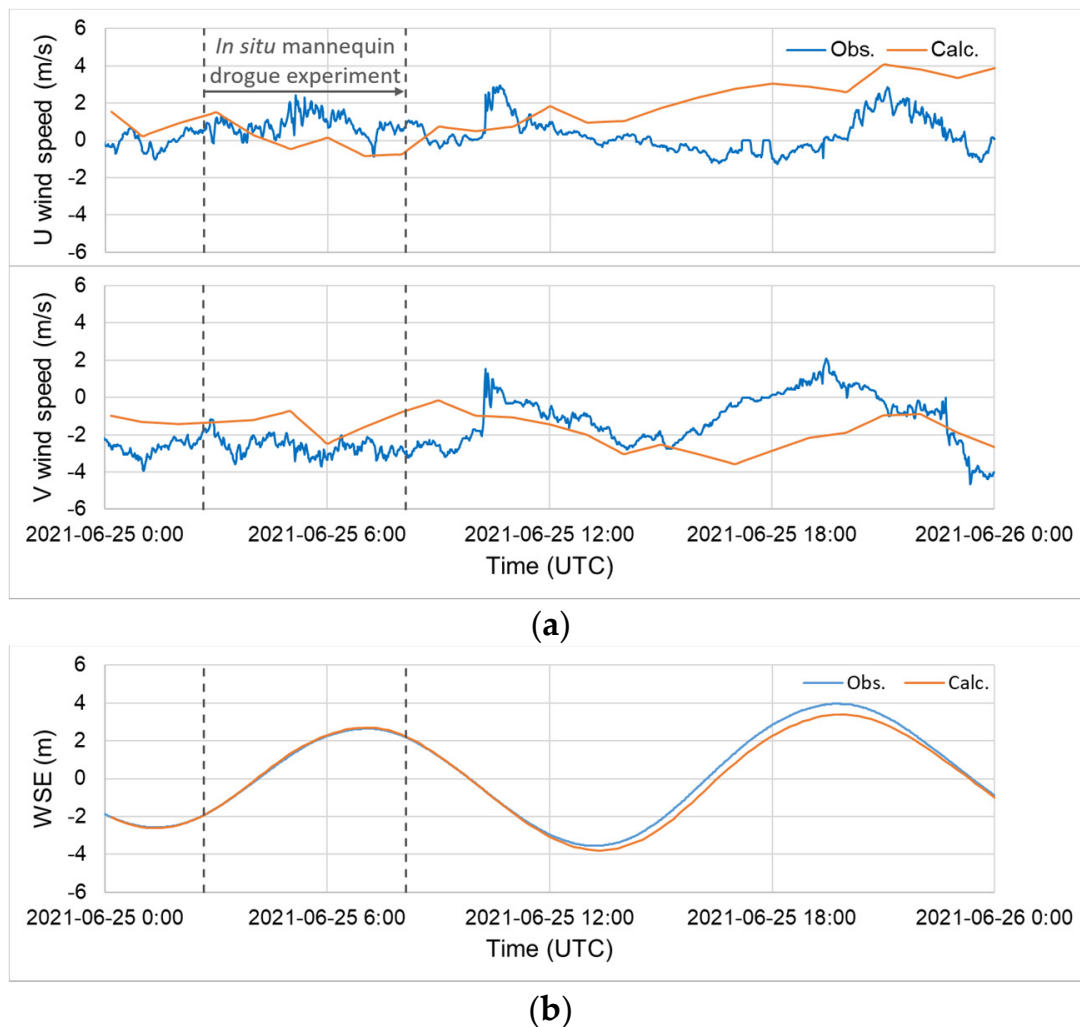


**Figure 10.** Comparison of wind speed (a) and water surface elevation (b) in Gadaeam and Taean (Figure 1).

#### 4.5. Probability in Finding Location

The usual SAR operations normally rely on deterministic approaches, that is, finding the location with respect to the movement of the missing float according to tidal excursion. However, in natural nonlinear interactions with tide, wind, and irregular bottom geomorphology, deterministic predictions could inaccurately identify a target point or search areas, thus misusing the golden time of rescue. Hence, in this study, we proposed a probabilistic approach by applying random-walk particle movements and the final location ratio from the release point. When particle tracking is performed backward, the source locations of an uncertain flow field can be found. Hammoud et al. [36] attempted to identify the release time and path of pollutants from fixed and moving sources using backward tracking.

Each floating neutral particle is affected by environmental tides, wind fields, and associated turbulent motion. Thus, sometimes the trajectories of particles expressed as  $x_i$  in Equation (1) show closed orbit probability due to random-walk characteristic and recursive tidal excursion.

The probabilistic location model of particle approach is widely adopted by oceanic accidental cases [8,10,37], particularly for instantaneous ship cracking or submergence oil spills. However, to the best of our knowledge, there is no coastal safety accident rescue modeling using probabilistic findings, especially under macro-tidal environments on tidal flats and along tidal channels.

In this study, we attempted to investigate the probability of SAR for an in situ mannequin test in the  $1 \times 1$  km detecting cell. Each cell has at least 5 (offshore) to 1316 (near coast) nodal points of unstructured grids. For each cell, portions of release particles were calculated at every computational time up to 12 h. According to the KCG report, this is known as a limit of golden time of rescue in normal coastal conditions. Simulated results as shown in Figure 11 (also provided in Supplementary Materials Video S3) clearly show that abrupt decrease of searching probability from the initial release point occurs after 6 h, when a half tidal excursion due to semi-lunar tidal constituent, distributes probability detection cell with low contents. Up to 6 h, cells with at least 50% of probability were partly detected. The reason for scattering of lower probability cells might be long tails of cells along the tidal motion due to macro-tidal environment. These results indicate that SAR for nearshore coastal accidents would be greatly influenced by local tidal motion; thus, in the SAR operational modeling local tidal motion should be fully considered. However, due to the distinctly different phenomena in the tidal area, modeling should be shifted in an appropriate manner to enhance the success of rescue missions within an golden time. Then, the approach can be extended to extreme weather conditions in real-time forecasting for rescue operations by the KCG.

In this study, we attempted to investigate the probability of SAR for an in situ mannequin test in the  $1 \times 1$  km detecting cell. Each cell has at least 5 (offshore) to 1316 (near coast) nodal points of unstructured grids. For each cell, portions of release particles were calculated at every computational time up to 12 h. According to the KCG report, this is known as a limit of golden time of rescue in normal coastal conditions. Simulated results as shown in Figure 11 (also provided in Supplementary Materials Video S3) clearly show that abrupt decrease of searching probability from the initial release point occurs after 6 h, when a half tidal excursion due to semi-lunar tidal constituent, distributes probability detection cell with low contents. Up to 6 h, cells with at least 50% of probability were partly detected. The reason for scattering of lower probability cells might be long tails of cells along the tidal motion due to macro-tidal environment. These results indicate that SAR for nearshore coastal accidents would be greatly influenced by local tidal motion; thus, in the SAR operational modeling local tidal motion should be fully considered. However, due to the distinctly different phenomena in the tidal area, modeling should be shifted in an appropriate manner to enhance the success of rescue missions within an golden time. Then, the approach can be extended to extreme weather conditions in real-time forecasting for rescue operations by the KCG.

As highlighted in several research reports, the term P (probability) in probability of containment (POC), probability of detection (POD), probability of search success (POS), or probability of rescue success (POR) [7,8,21,30] depends on diverse uncertainties in representing environmental forcing for a stochastic PTM, currents and winds, leeway characteristics for the search object, and horizontal dispersion required to account for the smaller subgrid scale turbulence and transport mechanisms [25]. We need to increase the probability by identifying each mechanism and minimizing the associated uncertainty by obtaining more information through sensitivity tests in further studies.

#### 4.6. Impact of Number of Particles on Accuracy and Computing Time

The total number of particles is a key factor to ensure accurate modeling of PTM. The importance of total number of particles in PTM is shown by the following aspects: (1) simulation of spreading throughout the domain of interest to estimate general movement, such as residence time of flushing rate between ocean and estuary; (2) continuous release of particles from a contaminant source point, such as a waste water treatment plant or thermal power plant; and (3) representation of a specific point of instantaneous accidents, such as oil spill, ship accidents, or marine leisure accidents that need SAR. The first two cases require relatively larger particles than that of the third case for capturing the whole transport pattern for the computation domain. Thus, for the purpose of SAR, the importance of total number of particles may be low.

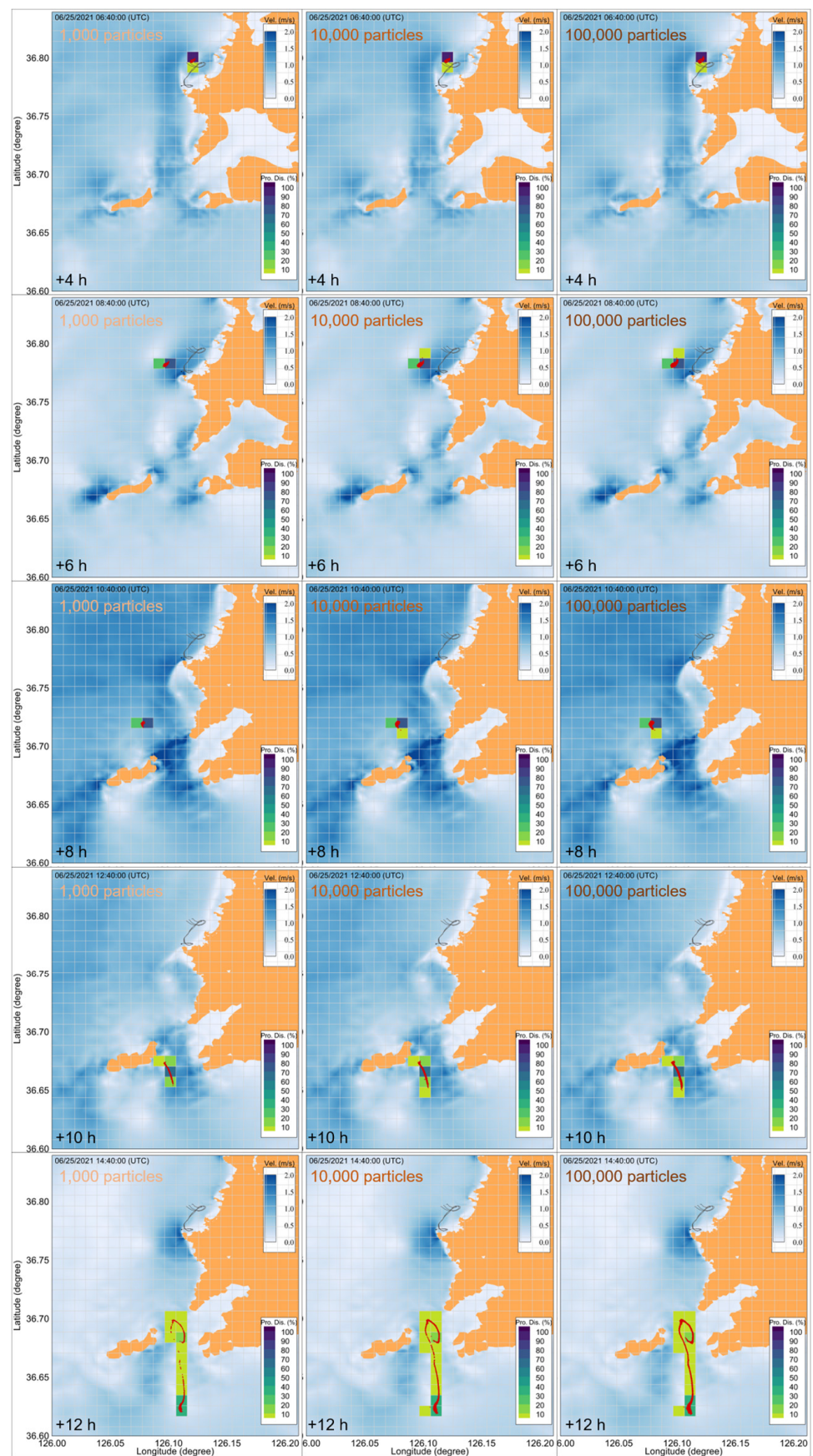


**Figure 11.** Temporal (elapsed time denoted as in the lower-left corner) probability distribution for the 1 × 1 km detecting cell of mannequin test.

It is generally expected that more particles result in higher accuracy. However, in the case of human accidents, if statistically sufficient particles [2] are used to satisfy a target accuracy, it is a plausible choice to maintain fast computing within a certain short time to meet EWS. Although setting the total number of particles targeting SAR is still debatable, Ličer [11] tested  $5 \times 10^3$  for a semi-active surfboard drift hindcasting simulation. In this study, we tested four cases by increasing the total number of particles to  $1 \times 10^3$ ,  $5 \times 10^3$ ,  $1 \times 10^4$ , and  $1 \times 10^5$  to capture the accuracy variation and computing time consumption. Although overall PTM coupled with ADCIRC can be performed using parallel computers, comparative tests were performed for 3 days of simulation on a single core 2.60 GHz Intel Xeon processor for comparison. In addition to the number of particles affecting the computation time, the time step of each particle movement is important for PTM. Although time steps of 1.0 and 0.2 s were set for idealized and real tests, respectively, the same as the time step in a hydrodynamics model in which a Lagrangian tracking scheme was applied, longer time steps of 60 and 10 min, respectively, were applied in postprocessing track particles. Nevertheless, the time step should be addressed to satisfy the particle Courant–Friedrichs–Lewy stability criterion in PTM, as suggested by Büyükçelebi et al. [3].

Simulation results showed almost the same probabilities for the initial 4 h of release time regardless of the total number of particles. When the elapsed time increased to 6 and 12 h, the probabilities for each case generally decreased. However, the differences were between 1% and 2% showing almost corresponding patterns of particle spreading. Computational time increased linearly from 2.9 to 172.6 min in accordance with larger particles from  $1 \times 10^3$  to  $1 \times 10^5$ , respectively. In addition, postprocessing time for visualization was not affected by the total particles, ranging from 1.5 to 2.4 min (Figure 12). Although the computation time depends on the simulation hardware, the linearly increasing trend with respect to number of particles was addressed by Mohtar et al. [20]. Thus, for an immediate operation, the  $1 \times 10^3$  particles demonstrated in this study were sufficient for SAR of EWS.

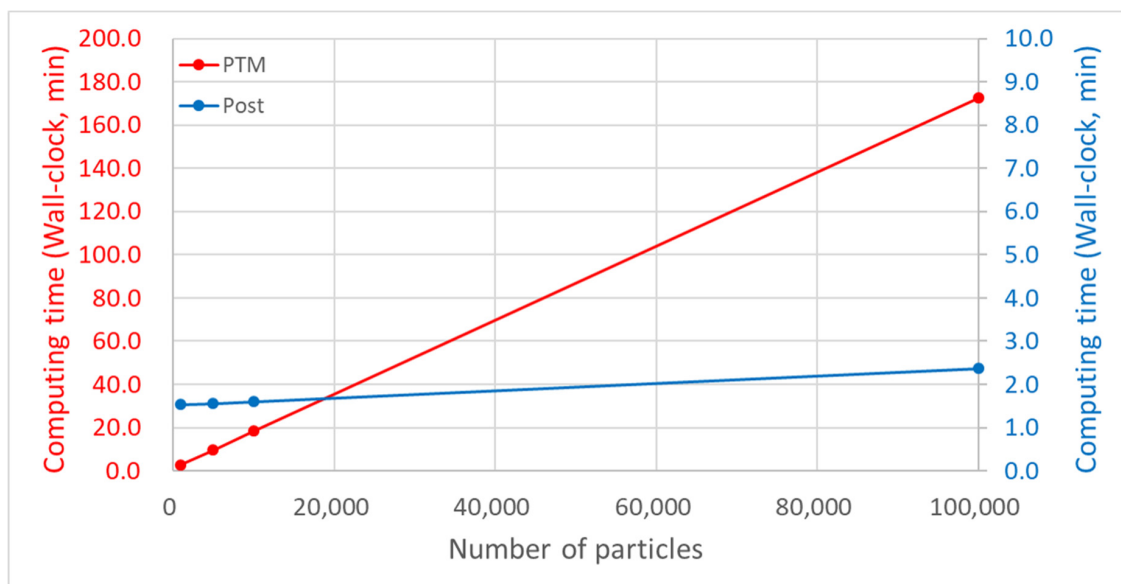


**Figure 12.** Comparison of CPU time (wall-clock) of particle tracking (red) and postprocessing (blue) for 1 day of simulation in accordance with number of particles.

#### 4.7. Importance of Genesis Time and Location in SAR

According to the SAR missions of the KCG, the uncertainties surrounding the initial location and time of missing persons greatly mislead the probability in actual rescue operations. To capture the final probability variations in accordance with the uncertainties surrounding the initial location and time, sensitivity tests were performed by shifting the location and time of missing persons. That is, missing locations were assumed just near the coast, with a deviation of 70 m from the original location and truncated to the third

decimal point of the latitude and longitude, matching it as the approximate location. To account for the uncertainty around the initial time persons went missing, we tested the shifting missing time as  $\pm 30$  and  $\pm 60$  min against the actual time. The simulated results in Figure 13 (Video S2) and Figure 14 (Video S4 and S5) show the differences that passed every hour with respect to the original time and location.

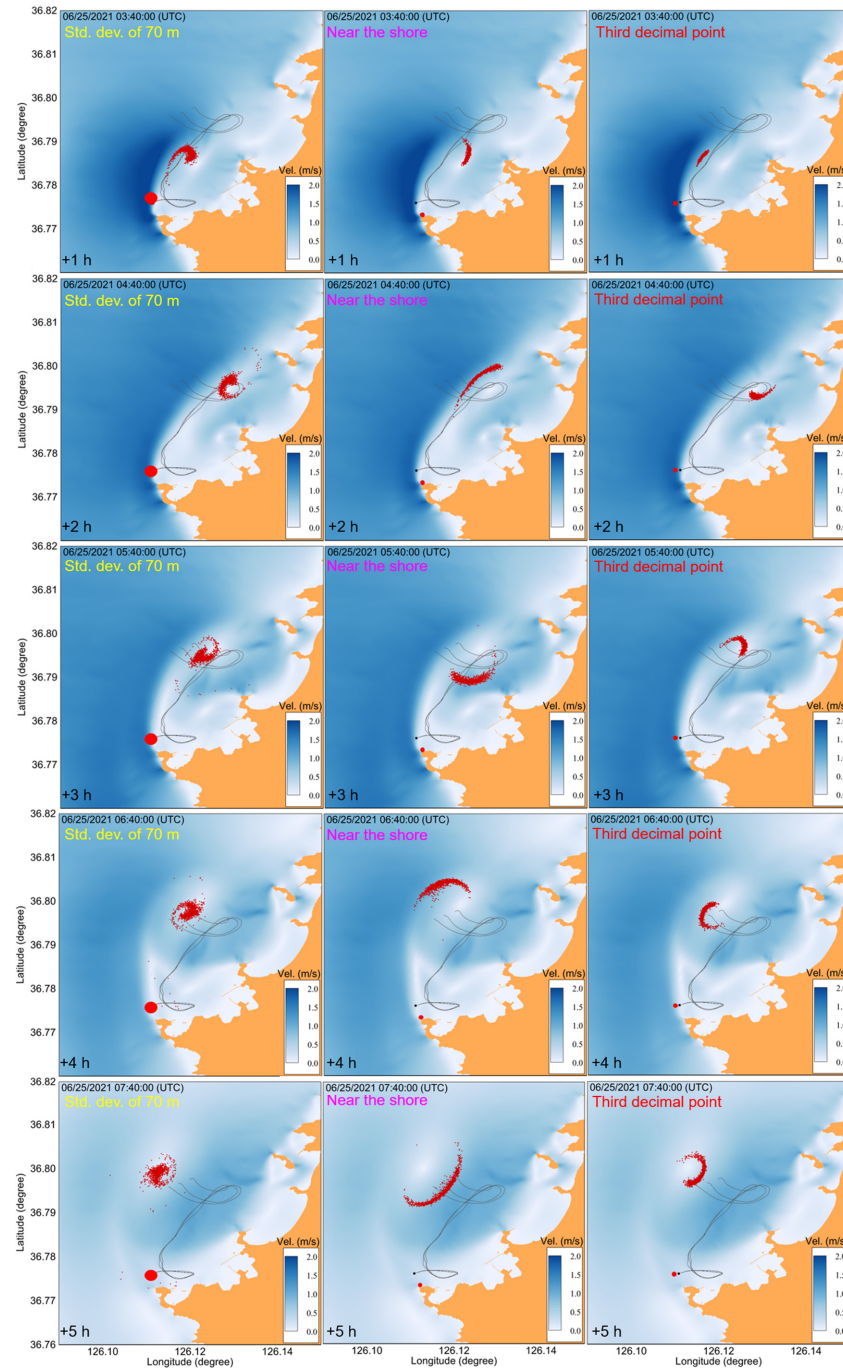


**Figure 13.** Simulated results depending on the source location of particle release after every hour of floating up to 5 h, overlapped on the black solid line of actual tracks (**left-panel**) shifted as a standard deviation of 70 m (**mid-panel**), intentionally locating near the shore, and (**right-panel**) input of uncertain coordinate as third decimal point truncation.

In the simulation of the in situ field experiments for mannequin floating tests, a total of 1000 particles were released to identify the remaining particles on a certain POC, which

moved according to the tidal flow direction, as defined in [8,10,37] with elapsed time from the source point.

As seen in Figure 14a, input of an accurate missing time greatly affected the entire SAR effort. For example, for a case occurring 30 min earlier, the location of particle clouds was near the particle release point, and thus the clouds of the particle only resided near the initial missing location for 1 h. However, within 2 h the clouds spread rapidly to the north according to the strong coastal currents and moved in a northeast direction at 3 h, reaching the coast and then moving forth and back, making long tails along the coast 4 and 5 h later, showing some stuck at shore and inland. However, at a 1 h earlier release time, the initial particle movement slightly deviated from the original point, the clouds were trapped and remained at the shore in a small bay for the entire 5 h elapsed simulation time.

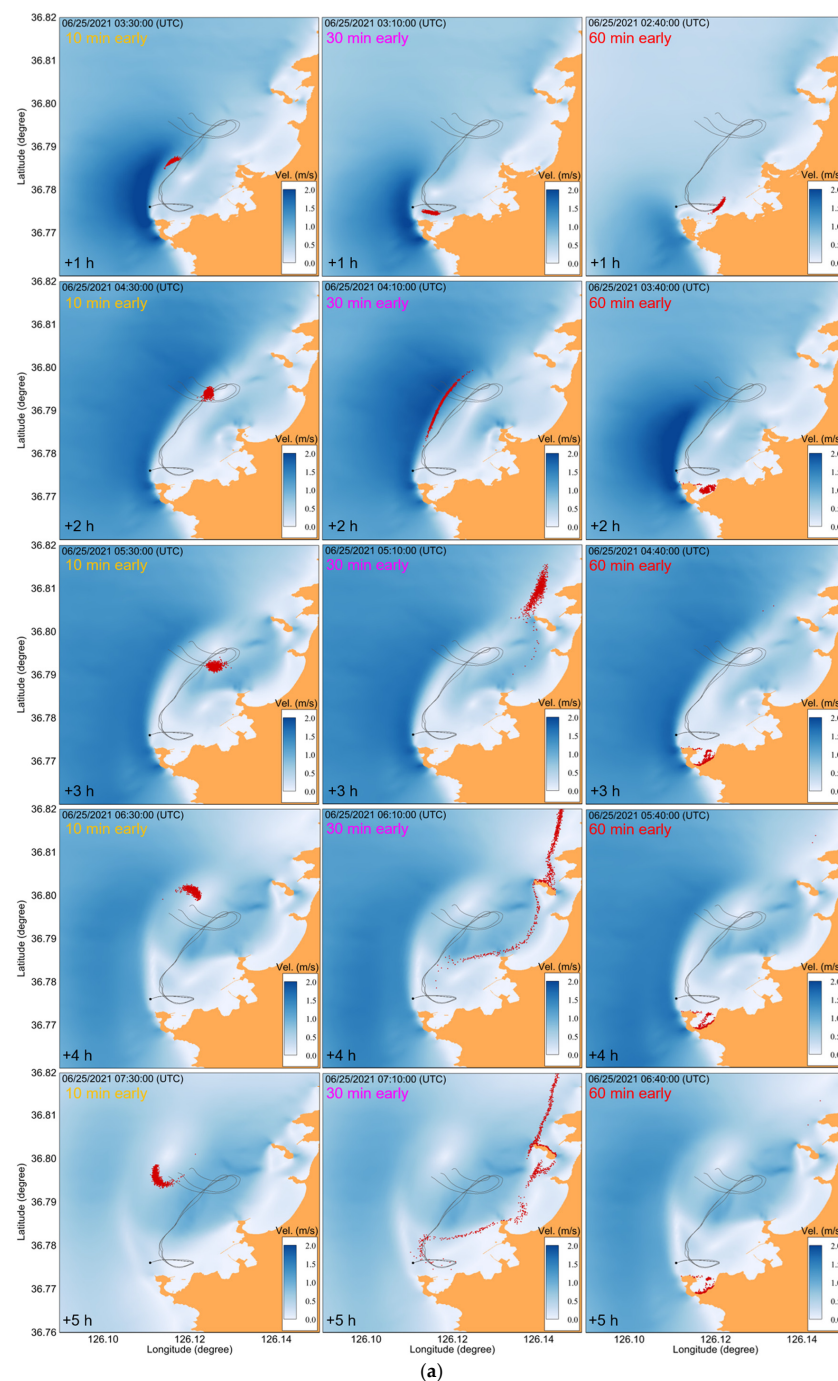
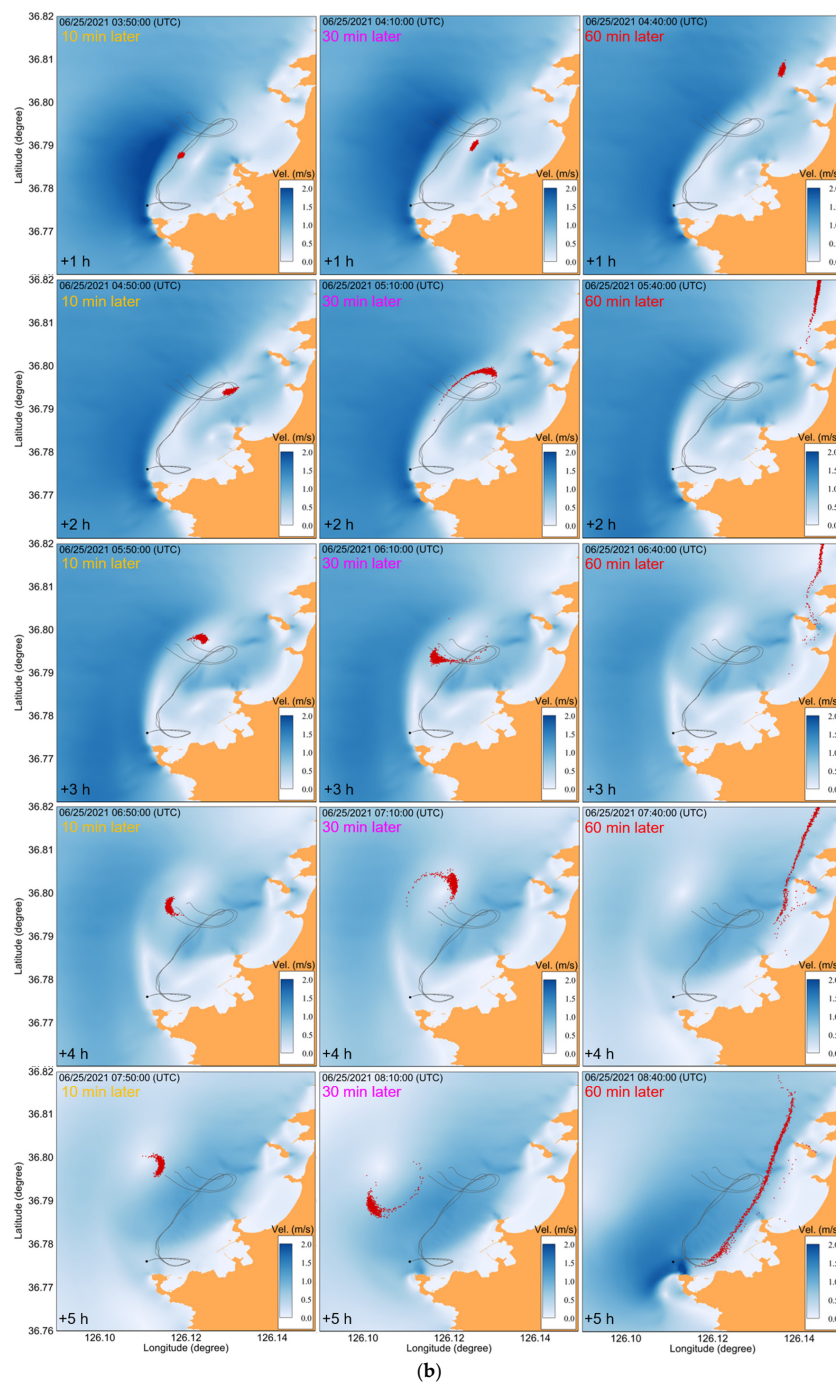


Figure 14. Cont.



**Figure 14.** Simulated results for up to 5 h of floating particle distribution by changing the particle release time, shifting it (a) earlier and (b) later, as noted in the upper left corner.

When the initial time was set to 30 and 60 min later than the actual missing time cases, the clouds moved far away in a northeast direction owing to the flooding currents, as shown in Figure 14b, even after 1 h of elapsed time. After 2 and 3 h, the clouds moved and resided near the target point of rescue in the case of 30 min later release; however, 1 h later, the clouds showed a narrow band along the farther shoreline, making it very difficult to limit the point of rescue (Figure 14). In addition, at 4 and 5 h, the spreading pattern showed further dispersion and additional shoreline sticking during the ebbing tide.

As anticipated, the simulated results after a 3 h simulation including all unknowns, presented a somewhat misleading rescue point, i.e., abrupt reduction of the “probability” term in SAR. Therefore, we need to obtain more accurate information on the initial missing

location to increase the accuracy of our predictions under a locally refined and discretized numerical model.

#### 4.8. Wind Effects

Among the external forces on the PTM, it was clear that the wind played an important role even in the near-coastal floating mechanism. This study aims to examine coastal accidents under severe weather conditions. Thus, sensitivity tests were conducted by increasing wind forcing to be comparable to the in situ mannequin field experiments. According to the analyzed annual wind field in the study area, the dominant direction and magnitude are northwest of 10 m/s with duration of 4 h. Hence, the simulation scenarios were provided with magnitudes ranging from 5 to 15 m/s with the wind factor. However, besides strong wind condition, a site-specific diurnal breeze wind effect during summer season is important but not included in the present study.

Simulation showed that the effects of wind on the floating material were significant when speeds exceeded 10 m/s, and as a result, some of the particles landed at the opposite end of the coast, but occasionally all were stuck to the shore (Figure 15 and Video S6). In the case of no-resurfacing due to mismatched tidal currents, there were only a few, that is, a very low probability of SAR in marine areas. This highlights the importance of providing real-time wind information for PTMs in operational SAR missions near the macro-tidal environments.

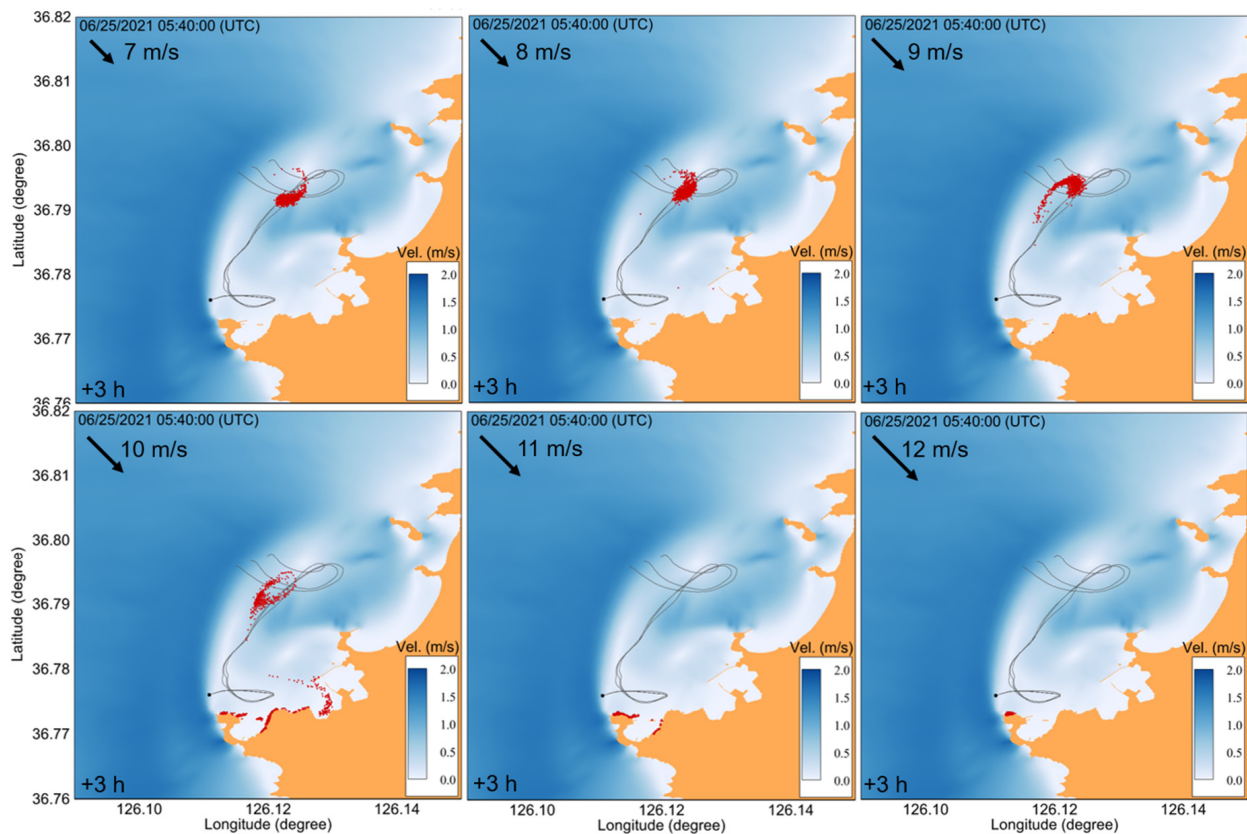


**Figure 15.** Simulated results depending on the wind effect on particle tracking after 3 h of floating; wind speeds are denoted in the upper-left corner of each map.

#### 5. Conclusions and Further Study

Marine leisure activities, such as fishing, swimming, yachting near coastal areas, and catching shelves in tidal flats, are rapidly increasing around the South Korean Peninsula, especially in the WCK due to increased accessibility from metro Seoul, the capital city. Accordingly, annual death toll resulting from safety accidents induced by impaired personal

recognition of external ascending tidal speeds on the very mild slope of tidal flats, and isolation and falling on slippery coastal rocks or tetrapods, are rising. To provide an adequate operational SAR strategy against nearshore accidents, finely resolved unstructured meshes accounting for wet–dry conditions applied to a wide range of tidal flats were discretized using the ADCIRC circulation model. A random-walk PTM was applied as a missing body floats, incorporating the surface drag effects as the leeway coefficient. Prior to field application, several sensitivity tests were performed to determine the important factors affecting SAR operations on the WCK. Our results showed that the accurate representation of the bottom slope and local bathymetry type were crucial, especially for nearshore leisure accident modeling. In particular, the bottom topography of the water depth in the offshore direction greatly affected the movement of coastal floats. Thus, it was very important to describe the bottom topography based on accurate water-depth data of the target simulation area. Moreover, turbulence due to tidal currents played an important role in the spreading mechanism. A recursive wet–dry in a macro-tidal condition showed quite different particle movements in normal offshore oil spills, vessel accidents, or marine debris transport.

Through numerical simulations, we found that the input of accurate timing of missing data played a major role in increasing the effective predictions of accident locations for SAR missions. Despite our findings, there remain several limitations and unknowns associated with these models, such as incorporating the time-varying buoyancy of missing body, minimizing ambiguity, partially resolving the present numerical approximation, and locally specifying the site-specific variant external wind forcing, which need to be elucidated in future studies.

**Supplementary Materials:** The following are available online at <https://www.mdpi.com/article/10.3390/jmse10030447/s1>, Video S1: Bottom slope and shape effect.wmv, Video S2: Source location.wmv, Video S3: Temporal probability changes.wmv, Video S4: Releasing time (earlier).wmv, Video S5: Releasing time (later).wmv, Video S6: Wind effect.wmv.

**Author Contributions:** Conceptualization, S.-W.S. and H.-J.K.; methodology, S.-W.S. and H.-J.K.; software, H.-J.K.; validation, S.-W.S. and H.-J.K.; data curation, H.-J.K.; writing—original draft preparation, S.-W.S. and H.-J.K.; writing—review and editing, S.-W.S. and H.-J.K.; visualization, H.-J.K.; supervision, S.-W.S. All authors have read and agreed to the published version of the manuscript.

**Funding:** This research was a part of a project titled “Integrated System Development of Risk Assessment and Prediction for Coastal Activity Areas”, funded by the Korea Coast Guard, Korea (20200527).

**Institutional Review Board Statement:** Not applicable.

**Informed Consent Statement:** Not applicable.

**Data Availability Statement:** Ocean tide model around Japan (NAO.99Jb model), [https://www.miz.nao.ac.jp/staffs/nao99/index\\_En.html](https://www.miz.nao.ac.jp/staffs/nao99/index_En.html) (accessed on 2 January 2022). Korea Hydrographic and Oceanographic Agency, <http://www.khoa.go.kr/oceangrid/khoa/koofs.do> (accessed on 2 January 2022); Korea Meteorological Administration, KMA Weather Data Service, Open MET Data Portal, <https://data.kma.go.kr/cmmn/main.do> (accessed on 2 January 2022).

**Conflicts of Interest:** The authors declare no conflict of interest.

## References

1. Seo, S.-N. Digital 30sec gridded bathymetric data of Korea marginal seas—KorBathy30s. *J. Korean Soc. Coast. Ocean Eng.* **2008**, *20*, 110–120. (In Korean)
2. Bilgili, A.; Proehl, J.A.; Lynch, D.R.; Smith, K.W.; Swift, M.R. Estuary/ocean exchange and tidal mixing in a Gulf of Maine Estuary: A Lagrangian modeling study. *Estuar. Coast. Shelf Sci.* **2005**, *65*, 607–624. [[CrossRef](#)]
3. Büyükçelebi, B.T.; Karabay, H.; Bilgili, A. Exchange characteristics of an anthropogenically modified lagoon: An Eulerian-Lagrangian modeling case study with an emphasis on the number of particles. *J. Environ. Eng. Landsc. Manag.* **2021**, *29*, 251–262. [[CrossRef](#)]
4. Eichhorn, M.; Haertel, A. A debris backwards flow simulation system for Malaysia airlines flight 370. In Proceedings of the OCEANS 2016, Shanghai, China, 10–13 April 2016. [[CrossRef](#)]

5. Kim, T.H.; Yang, C.S.; Oh, J.H.; Ouchi, K. Analysis of the contribution of wind drift factor to oil slick movement under strong tidal condition: Hebei Spirit oil spill case. *PLoS ONE* **2014**, *9*, e87393. [[CrossRef](#)]
6. Jung, T.S. Numerical simulation of spilled oil dispersion in Taean coastal zone. *J. Korean Soc. Mar. Environ. Energy* **2009**, *12*, 264–272. (In Korean)
7. Dietrich, J.C.; Trahan, C.J.; Howard, M.T.; Fleming, J.G.; Weaver, R.J.; Tanaka, S.; Yu, L.; Luettich, R.A.; Dawson, C.N.; Westerink, J.J.; et al. Surface trajectories of oil transport along the Northern Coastline of the Gulf of Mexico. *Cont. Shelf Res.* **2012**, *41*, 17–47. [[CrossRef](#)]
8. Xiong, W.; Van Gelder, P.H.A.J.M.; Yang, K. A decision support method for design and operationalization of search and rescue in maritime emergency. *Ocean Eng.* **2020**, *207*, 107399. [[CrossRef](#)]
9. Otote, D.A.; Li, B.; Ai, B.; Gao, S.; Xu, J.; Chen, X.; Lv, G. A decision-making algorithm for maritime search and rescue plan. *Sustainability* **2019**, *11*, 2084. [[CrossRef](#)]
10. Mou, J.; Hu, T.; Chen, P.; Chen, L. Cooperative MASS path planning for marine man overboard search. *Ocean Eng.* **2021**, *235*, 109376. [[CrossRef](#)]
11. Ličer, M.; Estival, S.; Reyes-Suarez, C.; Deponte, D.; Fettich, A. Lagrangian modelling of a person lost at sea during the Adriatic scirocco storm of 29 October 2018. *Nat. Hazards Earth Syst. Sci.* **2020**, *20*, 2335–2349. [[CrossRef](#)]
12. Suh, S.-W.; Lee, H.-Y. Analysis of hydrodynamic change around the Saemangeum area using a particle tracking method. *J. Korean Soc. Coast. Ocean Eng.* **2011**, *23*, 442–450. [[CrossRef](#)]
13. Suh, S.-W. A hybrid approach to particle tracking and Eulerian–Lagrangian models in the simulation of coastal dispersion. *Environ. Model. Softw.* **2006**, *21*, 234–242. [[CrossRef](#)]
14. Simons, R.D.; Siegel, D.A.; Brown, K.S. Model sensitivity and robustness in the estimation of larval transport: A study of particle tracking parameters. *J. Mar. Syst.* **2013**, *119–120*, 19–29. [[CrossRef](#)]
15. George, G.; Vethamony, P.; Sudheesh, K.; Babu, M.T. Fish larval transport in a macro-tidal regime: Gulf of Kachchh, west coast of India. *Fish. Res.* **2011**, *110*, 160–169. [[CrossRef](#)]
16. Hinata, H.; Sagawa, N.; Kataoka, T.; Takeoka, H. Numerical modeling of the beach process of marine plastics: A probabilistic and diagnostic approach with a particle tracking method. *Mar. Pollut. Bull.* **2020**, *152*, 110910. [[CrossRef](#)] [[PubMed](#)]
17. Seo, S.; Park, Y.-G. Destination of floating plastic debris released from ten major rivers around the Korean Peninsula. *Environ. Int.* **2020**, *138*, 105655. [[CrossRef](#)] [[PubMed](#)]
18. Yoon, J.-H.; Kawano, S.; Igawa, S. Modeling of marine litter drift and beaching in the Japan Sea. *Mar. Pollut. Bull.* **2010**, *60*, 448–463. [[CrossRef](#)]
19. Isobe, A.; Kako, S.; Chang, P.-H.; Matsuno, T. Two-way particle-tracking model for specifying sources of drifting objects: Application to the East China Sea Shelf. *J. Atmos. Ocean. Technol.* **2009**, *26*, 1672–1682. [[CrossRef](#)]
20. Mohtar, S.E.; Hoteit, I.; Knio, O.; Issa, L.; Lakkis, I. Lagrangian tracking in stochastic fields with application to an ensemble of velocity fields in the Red Sea. *Ocean Modell.* **2018**, *131*, 1–14. [[CrossRef](#)]
21. Allen, A.; Roth, J.-C.; Maisondieu, C.; Breivik, Ø.; Forest, B. *Field Determination of the Leeway of Drifting Objects, The Leeway of a 20-ft Container, WWII Mine, Skiff, Sunfish, and a PIW in the Deceased Position*; Norwegian Meteorological Institute: Fedje, Norway; Andfjord, Norway, 2010; p. 43.
22. Kako, S.; Isobe, A.; Seino, S.; Kojima, A. Inverse estimation of drifting-object outflows using actual observation data. *J. Oceanogr.* **2010**, *66*, 291–297. [[CrossRef](#)]
23. Breivik, Ø.; Allen, A.A.; Maisondieu, C.; Roth, J.C. Wind-induced drift of objects at sea: The leeway field method. *Appl. Ocean Res.* **2011**, *33*, 100–109. [[CrossRef](#)]
24. Brushett, B.A.; Allen, A.A.; Futch, V.C.; King, B.A.; Lemckert, C.J. Determining the leeway drift characteristics of tropical Pacific island craft. *Appl. Ocean Res.* **2014**, *44*, 92–101. [[CrossRef](#)]
25. Brushett, B.A.; Allen, A.A.; King, B.A.; Lemckert, C.J. Application of leeway drift data to predict the drift of panga skiffs: Case study of maritime search and rescue in the tropical pacific. *Appl. Ocean Res.* **2017**, *67*, 109–124. [[CrossRef](#)]
26. Richardson, P.L. Drifting in the wind: Leeway error in shipdrift data. *Deep Sea Res. Part I Oceanogr. Res. Pap.* **1997**, *44*, 1877–1903. [[CrossRef](#)]
27. Zhang, J.; Teixeira, Â.P.; Soares, C.G.; Yan, X. Probabilistic modelling of the drifting trajectory of an object under the effect of wind and current for maritime search and rescue. *Ocean Eng.* **2017**, *129*, 253–264. [[CrossRef](#)]
28. Korea Research Institute of Ships & Ocean Engineering (KRISO). *Understanding of Floating Marine Litter Distribution in the NOWPAP Region*; Korea Research Institute of Ships & Ocean Engineering: Daejeon, Korea, 2017; p. 58.
29. Critchell, K.; Grech, A.; Schlaefer, J.; Andutta, F.P.; Lambrechts, J.; Wolanski, E.; Hamann, M. Modelling the fate of marine debris along a complex shoreline: Lessons from the Great Barrier Reef. *Estuar. Coast. Shelf Sci.* **2015**, *167*, 414–426. [[CrossRef](#)]
30. Luettich, J.R.; Westerink, J.; Scheffner, N. *ADCIRC: An Advanced Three-Dimensional Circulation Model for Shelves, Coasts, and Estuaries. Report 1. Theory and Methodology of ADCIRC-2DDI and ADCIRC-3DL*; Department of the Army US Army Corps of Engineers: Washington, DC, USA, 1992; p. 137.
31. Suh, S.-W.; Lee, H.-Y.; Kim, H.-J.; Fleming, J.G. An efficient early warning system for typhoon storm surge based on time-varying advisories by coupled ADCIRC and SWAN. *Ocean Dyn.* **2015**, *65*, 617–646. [[CrossRef](#)]
32. Salamon, P.; Fernández-García, D.; Gómez-Hernández, J.J. A review and numerical assessment of the random walk particle tracking method. *J. Contam. Hydrol.* **2006**, *87*, 277–305. [[CrossRef](#)] [[PubMed](#)]

33. Suh, S.-W.; Lee, H.-Y.; Kim, H.-J. Spatio-temporal variability of tidal asymmetry due to multiple coastal constructions along the West Coast of Korea. *Estuar. Coast. Shelf Sci.* **2014**, *151*, 336–346. [[CrossRef](#)]
34. Matsumoto, K.; Takanezawa, T.; Ooe, M. Ocean tide models developed by assimilating TOPEX/POSEIDON altimeter data into hydrodynamical model: A global model and a regional model around Japan. *J. Oceanogr.* **2000**, *56*, 567–581. [[CrossRef](#)]
35. Jalón-Rojas, I.; Wang, X.H.; Fredj, E. A 3D numerical model to Track Marine Plastic Debris (TrackMPD): Sensitivity of microplastic trajectories and fates to particle dynamical properties and physical processes. *Mar. Pollut. Bull.* **2019**, *141*, 256–272. [[CrossRef](#)] [[PubMed](#)]
36. Hammoud, M.A.E.R.; Lakkis, I.; Knio, O.; Hoteit, I. Moving source identification in an uncertain marine flow: Mediterranean Sea application. *Ocean Eng.* **2021**, *220*, 108435. [[CrossRef](#)]
37. Ai, B.; Li, B.; Gao, S.; Xu, J.; Shang, H. An intelligent decision algorithm for the generation of maritime search and rescue emergency response plans. *IEEE Access* **2019**, *7*, 155835–155850. [[CrossRef](#)]